Analysis of bypass transition process using large eddy simulations

Adèle Veilleux, Loïc Jecker, Olivier Vermeersch, Hugues Deniau

Association Aéronautique et Astronautique de France

56th 3AF International Conference on Applied Aerodynamics
28 — 30 March 2022, Toulouse – France

FP50-AERO2022-veilleux

ANALYSIS OF BYPASS TRANSITION PROCESS USING LARGE EDDY SIMULATIONS

A. Veilleux [(1)], L. Jecker[(2)], O. Vermeersch[(3)] and H. Deniau[(4)]

[(1)]*Ph.D., ONERA DMPE, 2 av. Edouard Belin, 31055 Toulouse, France, Adele.Veilleux@onera.fr*

[(2)]*Ph.D., ONERA DMPE, 2 av. Edouard Belin, 31055 Toulouse, France, Loic.Jecker@onera.fr*

[(3)]*Ph.D., ONERA DMPE, 2 av. Edouard Belin, 31055 Toulouse, France, Olivier.Vermeersch@onera.fr*

[(4)]*Ph.D., ONERA DMPE, 2 av. Edouard Belin, 31055 Toulouse, France, Hugues.Deniau@onera.fr*

ABSTRACT

This paper describes the setup of a wall-resolved large eddy simulation (LES) of bypass transition on a realistic flat plate and the results obtained. This simulation is the first to compute a bypass transition flow on a flat plate from the receptivity stage to the laminar-turbulent transition onset. The key mechanisms of bypass transition are highlighted by the simulation: the shear-sheltering, the birth of Klebanoff-modes, their amplification, and destabilization.

1. INTRODUCTION

1.1 Bypass Transition Mechanism

The understanding of the laminar-to-turbulent transition phenomena is of strong interest as it occurs in many aerodynamics flows and strongly impacts the performances of aeronautical devices like aircraft wings or turbine blades. An accurate prediction of the transitional flow properties is thus essential. Depending on the flow configuration, transition to turbulence can follow different paths. In a boundary layer submitted to energetic freestream turbulence (FST), streak-shaped instabilities appear, grow and trigger the transition. Streaks were first described by Klebanoff [1] and called Klebanoff-modes by Kendall [2]. Klebanoff-modes are long streamwise streaks with small spanwise scales propagating within the boundary layer while the boundary layer remains laminar. They are associated with low frequencies and a strong amplitude, approximately 10% of the external velocity. This scenario is called bypass transition and is particularly difficult to model. The bypass transition scenario observes the following stages:

1. During the receptivity phase, external perturbations penetrate the laminar region of the boundary layer leading to the birth of streaks;
2. Streaks are generated and strongly amplified during a linear growth phase;
3. Streaks are destabilized during a non-linear phase and lead to the formation of turbulent spots;
4. Turbulent spots spread in the boundary layer, which becomes fully turbulent.

1.2 Previous experimental and numerical work

Bypass transition has been studied through experiments. The reference is the one from Roach *et al.* [3], where the mean and fluctuating velocities were measured on a flat plate submitted to a grid turbulence ($0.9\% < Tu < 6\%$) with and without a pressure gradient. Jonáš *et al.* [4] reproduced a similar experiment, without pressure gradient but with different turbulence length scales. They observed that when increasing the free-stream turbulence length scale, the onset of transition moved upstream and the transition region becomes longer. Other authors provide qualitative results [5, 6, 7], but not such quantitative data.

From a numerical point of view, few realistic simulations are available. The first LES was performed by Voke and Yang in 1995 [8]. Although under-resolved, their simulation demonstrates the prominent role of the wall-normal velocity fluctuation of the external turbulence in the streaks formation process. Jacobs and Durbin realized

a well-resolved DNS of flat plate submitted to external turbulence [9]. To lighten the mesh, the domain inflow is located downstream of the leading edge. The turbulence is then generated with a sum of Orr-Sommerfeld modes decaying toward the wall. The receptivity stage is thus not taken into account. They propose one bypass scenario where backward streaks move up in the boundary layer and provide a receptivity path between the free-stream turbulence high frequencies and the boundary layer. In this scenario, streaks are destabilized by external perturbations and there is thus no evidence of inherent streak instability. Brandt *et al.* run a similar DNS [10] which led them to proposed an alternative scenario based on the existence of secondary instabilities where streaks destabilization originates from two types of instability modes of low-speed streaks (the sinuous and the varicose modes of instability).

In all the above mentioned simulations [8, 9, 10], the leading-edge region is not treated and thus the receptivity process is not taken into account. To the authors knowledge, the only studies including the receptivity region in bypass transition are those from Nagarajan *et al.* [11] and Ovchinnikov *et al.* [12]. Their study demonstrates the influence of the leading edge on the generation of disturbances in the boundary layer. They use a super-ellipse type leading edge with an aspect ratio of 6 or 10 very similar to the one used in this study, but with a size that would not allow to easily reproduce the configuration experimentally. The Reynolds number based on the leading-edge radius and the upstream velocity is equals to $Re_r = 470$ in the study of Ovchinnikov *et al.* [12] and $5000 < Re_r < 8400$ in the study of Nagarajan *et al.* [11]. In the current study, this number is equal to $Re_r = 34000$, that is to say at least one order of magnitude greater than in previous simulations.

1.3 Aim of the present work

A bypass-transition model for Reynolds Averaged Navier Stokes (RANS) applications has been developed at ONERA [13]. However, this model has two main limitations: the representation of the FST penetration into the boundary layer is not accurate and the transition dynamic relies on macroscopic considerations. To model these two aspects of bypass transition more accurately, there is a need for data. This study thus consists in simulating the entire bypass transition process on a realistic flat plate with the wall resolved Large Eddy Simulation (LES) method.

The global context of this study is to realize a bypass transition experiment in a wind tunnel while simulating the very same configuration. LES is a very powerful tool that allows having access to quantities in particular in the receptivity zone and the transitional region. However, very long and costly simulations are necessary to be well-resolved at low frequencies. Since experiments are associated with longer acquisition times, getting low frequencies information is easier and less expensive in time. The aim is thus to use both the experimental and numerical approaches in a complementary way to better understand the bypass transition phenomenon. Both adiabatic and cooled walls will be tested because of the destabilizing effect of a cold wall on streaks suggested by the Optimal Perturbation Theory (OPT) [14, 15, 16]. The leading edge must be thick enough to use a cooling device in the experiment, thus a 3 cm thick leading edge was chosen. The experimental work is conducted at ONERA by Daswani *et al.* [17]. In this paper, only the LES results of bypass transition over an adiabatic wall are presented.

2. NUMERICAL SET-UP

2.1 Flat-plate configuration

The simulated flat plate has an elliptical leading edge with a radius of 15 mm and an aspect ratio of 10, leading to a length of 150 mm. The Mach number of the upstream flow is $M = 0.1$, with a turbulence level of $Tu \sim 6\%$ on the leading edge and a turbulence length scale of $\Lambda_T = 0.01$m.

2.2 Simulation configuration

The simulation is run with the compressible CFD code elsA [18] developed at ONERA. The general strategy of the simulation is the following.

1. A 2D RANS simulation provides the base flow on an extended domain;
2. A 2D 'box' is extracted from this domain, extruded in the transverse direction, and re-meshed in order to run a wall resolved LES;
3. The 3D LES is computed. Once the permanent regime is reached, a physical time of $t_f = 5.38 \cdot 10^{-2}$s was computed.

2.3 Numerical scheme and filter

The spatial scheme is based on a low-dispersion and low-dissipation compact scheme of Lele [19], adapted to a 5^{th}-order finite volume formulation [20]. A high-order filter of Visbal *et al.* [21] is used for two purposes: filter the unresolved waves and serve as a sub-grid model for the LES (which is then an implicit LES). The time integration is explicitly realized by a 6-steps Runge-Kutta scheme developed by Bogey *et al.* [22].

2.4 Mesh

The size of the simulation's domain has to be large enough to inject physically representative turbulence.

Moreover, a wall resolved LES strongly constrains the size of cells at the wall. The size of cells at the wall is formulated in "wall variables" dx_i^+:

$$dx_i^+ = \frac{dx_i}{l_\nu} = \frac{dx_i u_\tau}{\nu} \quad \text{with} \quad u_\tau = \sqrt{\frac{\tau_w}{\rho}}, \qquad (1)$$

where ρ is the fluid density and τ_w is the wall shear stress. A literature study showed that the constraints on the size of the cells are stronger in bypass transition than for a fully turbulent flow [9, 11, 12]. However, the use of a high-order scheme enables to release the constraint in the streamwise direction to $dx^+ \sim 40$ [11], compared to $dx^+ \sim 10$ with a 2nd-order scheme [9, 12]. In this simulation, at the wall, $dx^+ \in [5,18]$, $dy^+ \leq 2$ and $dz^+ \sim 3$ in the streamwise, wall-normal and spanwise directions. The mesh has a final size of $2401 \times 501 \times 325$ points in the directions $(\vec{x},\vec{y},\vec{z})$ respectively.

2.5 Boundary conditions and initialization

A non-radiative boundary condition developed by Tam *et al.* [23] is used to impose the RANS solution on the external frontier. An NSCBC condition (Navier-Stokes Characteristic Outflow Boundary Conditions, Poinsot *et al.* [24]) is used on the outflow to impose the pressure on this frontier. The initial state is given by the laminar RANS results. A key element of the simulation is the turbulence injection. Homogeneous isotropic turbulence is injected on the inflow of the domain with the method of Bechara *et al.* [25]. A fluctuating velocity field is built with a finite number of Fourier modes. The energy of each mode is determined with a von Kármán spectrum [26]. This fluctuating velocity field is added to the inflow velocity through the Tam *et al.* condition.

3. RESULTS

3.1 Definitions

During the simulation, several quantities are extracted:

- Time averaged values containing $\overline{u_i}, \overline{u_i u_j}$ with $u_i = (u,v,w)$. From those time-averaged values, root-mean-square values are computed as:

  $$u_{i,rms} = \sqrt{\overline{u_i^2} - (\overline{u_i})^2}$$

  And a 2D time-averaged and transverse-averaged mean flow is computed as:

  $$\tilde{u_i'}(x,y) = \frac{1}{L_z}\int_{-L_z/2}^{L_z/2} u_{i,rms}(x,y,z)dz$$

- Instantaneous data containing $u_i(x,y,z,t)$ on probes (every 100 iterations) and for the entire field (every 7520 iterations). Series of probes are distributed on the plate (at several fixed x,y), in the boundary layer (at several fixed z) and in the freestream. From instantaneous data, velocity fluctuations are computed as:

  $$u_i'(x,y,z,t) = u_i(x,y,z,t) - \overline{u_i}(x,y,z)$$

Through a geometric transformation, each quantity can be expressed from the coordinate system $(\vec{x},\vec{y},\vec{z})$ to a coordinate system local to the flat plate noted $(\vec{l},\vec{n},\vec{z})$ illustrated in Fig. 1(a). In the flat plate local coordinate system, the time-transverse-averaged values $\tilde{u_i'} = (\tilde{u'},\tilde{v'},\tilde{w'})$ are noted $(\tilde{u_l'},\tilde{v_n'},\tilde{w'})$ and the fluctuations $u_i' = (u',v',w')$ computed from instantaneous data are noted (u_l',v_n',w').

3.2 Receptivity region

Streaks originate from the penetration of external perturbations into the laminar region of the boundary layer during the receptivity phase. The analysis of the phenomena occurring in the receptivity region is therefore essential to better understand the generation of streaks.

3.2.1 Evaluation of the injected turbulence

Time-transverse-averaged turbulence intensities in each direction are computed in the flat plate local coordinate system as:

$$Tu_l = \frac{\tilde{u_l'}}{U_e}, \quad Tv_n = \frac{\tilde{v_n'}}{U_e}, \quad Tw = \frac{\tilde{w'}}{U_e},$$

$$Tt_p = \frac{\sqrt{(\tilde{u_l'}^2 + \tilde{v_n'}^2 + \tilde{w'}^2)/3}}{U_e},$$

and plotted in Fig. 1 at the boundary layer edge ($\eta_{99} = y/\delta_{99} = 1$) and for a wall distance $\Delta y = 1.2$cm. Strong anisotropy of the turbulence is observed at the boundary-layer edge in Fig. 1(b). This anisotropy is mainly explained by the damping of the wall-normal component of the turbulence close to the wall. By plotting turbulence intensities further away from the wall, at $\Delta y = 1.2$cm, the flow is no longer disturbed by the influence of the leading edge, and better properties can be observed in Fig. 1(c). The streamwise and wall-normal components show the same behavior and the same levels of turbulence intensity; the spanwise component, however, is still lower. The injected turbulence is thus not fully isotropic.

3.2.2 Vortices exciting the boundary layer

Fig. 2 shows vortices of the FST impacting the leading edge. They are identified in green by iso-surfaces of Q-criterion. Most upstream vortices have a vertical direction. When approaching the plate, the vortices direction aligns with the wall as observed by Nagarajan [11]. These

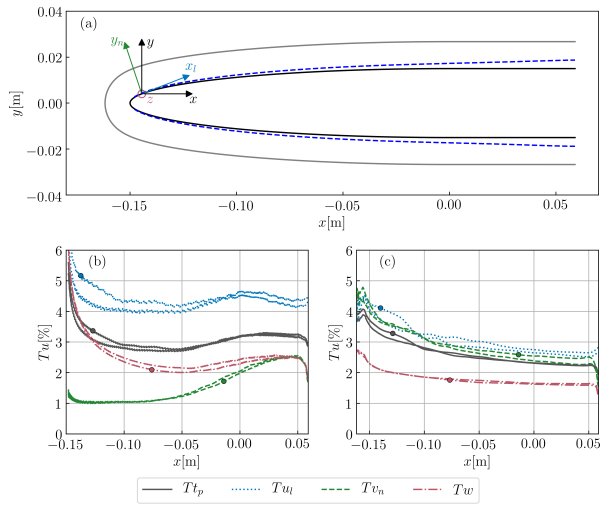

Figure 1: (a) Visualisation of the flat plate (—), $\eta_{99} = 1$ (– –), $\Delta y = 1.2$cm (—). (b,c) Turbulence intensities of the time-transverse-averaged mean flow at $\eta_{99} = 1$ (left) and $\Delta y = 1.2$cm (right). The marker (○) indicates the extrado ($y > 0$).

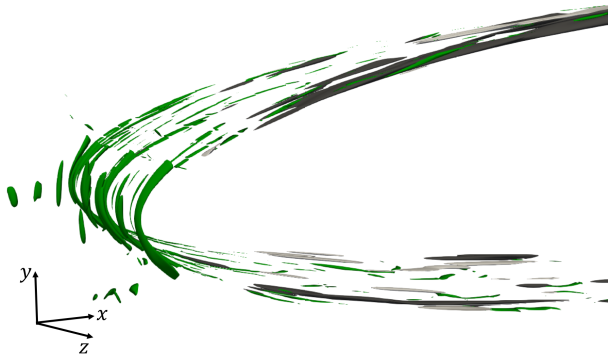

Figure 2: Iso-surfaces of the streamwise velocity disturbances u'_l and Q-criterion at $t = 1.40 \cdot 10^{-3}$s ($u'_l = -4$m/s in black, $u'_l = 4$m/s in grey and $Q = 1.8 \cdot 10^7 \text{s}^{-2}$ in green).

vortices, situated at the boundary-layer edge, feed the receptivity process.

This process can also be observed by plotting the time-transverse-averaged streamwise and normal velocity fluctuations at different positions in front of the leading edge. As we get closer to the leading edge, $\tilde{u}'$ increases around $y = (-0.0025, 0.0025)$ and decreases at $y = 0$, showing a clear peak. At the same position ($y = 0$), $\tilde{v}'$ strongly increases: the initial value $\tilde{v}' \sim 1$m/s at $x = -0.165$m has doubled at $x = -0.151$m. The increase of the wall-normal velocity fluctuations in the receptivity region is a key factor in the birth stage of the streaks. This component is involved in the lift-up mechanism [27, 28] which consists in a coupling between the wall-normal velocity fluctuation and the mean-flow shear, leading to streak-

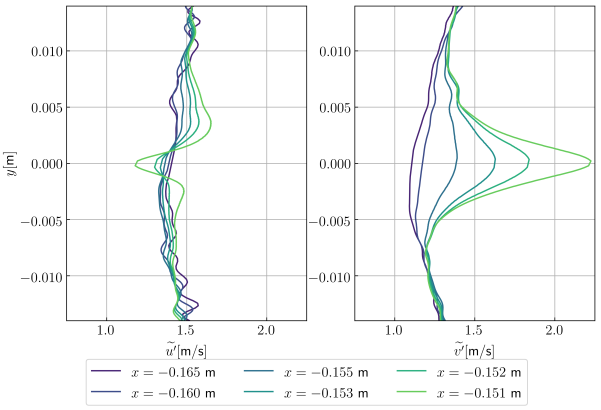

Figure 3: Evolution of the time-transverse-averaged streamwise and normal velocity fluctuations at different positions in front of the leading edge.

shaped streamwise disturbances formation and growth: the Klebanoff-modes.

3.3 Analysis of the time-transverse-averaged flow

To better understand the different steps involved in the bypass transition process, the time-transverse-averaged flow is analyzed. Boundary-layer integral values are computed: the shape factor, the friction coefficient, and the boundary-layer thickness are displayed in Fig. 4. The friction coefficient is compared to a Blasius and a theoretical turbulent streamwise evolution profile. The onset of the transition is located around $x = 0.07$cm, corresponding to the location where the friction coefficient starts to increase away from the Blasius profile (in red). This location is highlighted in the figure with a vertical black line and will be denoted x_{tr}. A fully-turbulent state is not reached since the friction coefficient does not increase up to the turbulent profile (in blue). The transition position x_{tr} can also be seen from the evolution of the shape factor H_{12}, which begins to decreases faster, and on the boundary-layer thickness evolution (Fig. 4b). In particular, the displacement thickness δ_1 follows a law in $\sqrt{x}$ until x_{tr} and becomes linear for $x > x_{tr}$ and the growth of δ_{99} is suddenly faster. Another location of interest is the abscissa $x = -7.84$cm corresponding to the maximum value of the shape factor, denoted $x_{H_{12}}$. This position can be retrieved on the evolution of δ_{99}, which follows a $x^b, b = 0.57$ law while $x < x_{H_{12}}$ but growth too fast and leaves this law for $x > x_{H_{12}}$. Since Klebanoff-modes are streamwise disturbances, a quantity of interest to better understand their evolution along with the flat plate (birth, amplification, and destabilization) is the maximal value of the time-space-averaged streamwise fluctuation $\tilde{u}'_l$ within the boundary layer. The evolution of $\tilde{u}'_{l,max}/U_e$ is plotted in Fig. 5 (solid black line) as well as the height

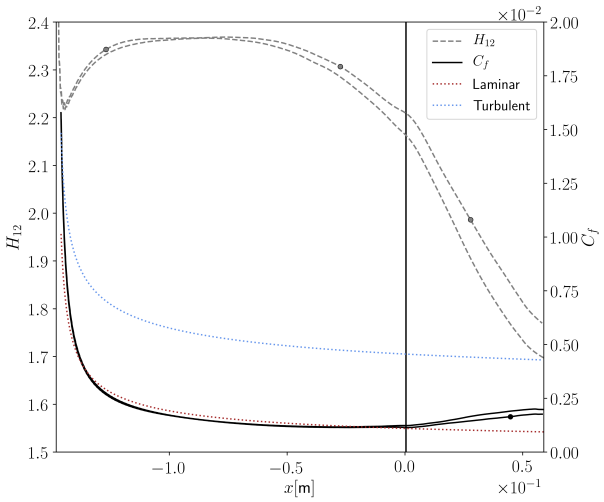

(a) Shape factor H_{12} and friction coefficient C_f.

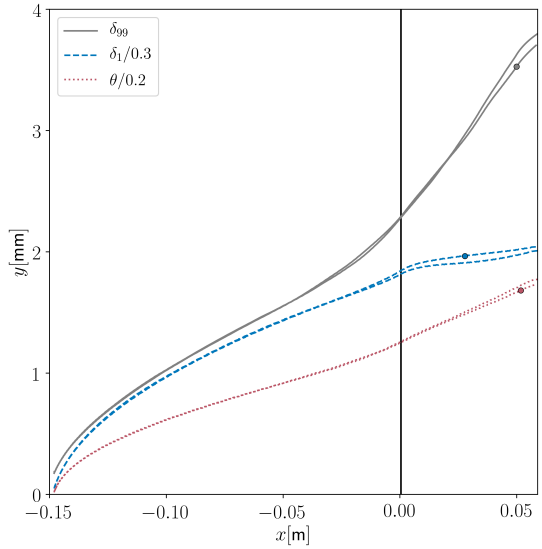

(b) Boundary-layer thickness

Figure 4: Shape factor H_{12}, friction coefficient C_f and boundary-layer thickness of the time-transverse-averaged mean flow along the plate. The marker (○) indicates the extrado ($y > 0$).

of this maximum in the boundary layer (dashed grey line). The maximum of $\widetilde{u'_l}/U_e$ growths from 8% to 10% of the external velocity up to the location $x_d = -2.48$cm. For $x > x_d$, the growth becomes faster and reaches 17% of the external velocity. This evolution indicates that streaks have an amplitude of $\sim 9\%$ of the external velocity which slowly amplified up to x_d, from where they are destabilized. Regarding their position in the boundary layer, their maximal value in the boundary layer thickness is first located at $\eta_{99} = 0.45$, as predicted by the OPT [29]. During the amplification phase, the maximum slowly goes down at $\eta_{99} = 0.35$. At $x = x_d$, it suddenly gets low in the boundary layer up to $\eta_{99} = 0.1$.

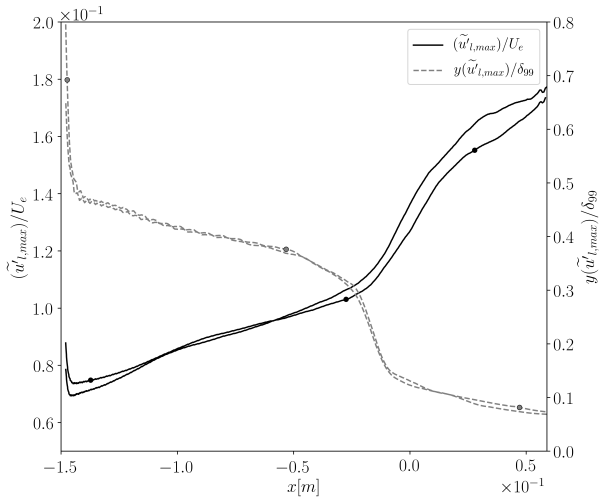

Figure 5: Maximum of $\widetilde{u'_l}/U_e$ and its position

Fig. 6 depicts time-transverse-averaged velocity-fluctuation profiles ($\widetilde{u'}_l, \widetilde{u'}_l/\max(\widetilde{u'}_l), \widetilde{v'}_n$ and $\widetilde{w'}$) for 14 abscissa from the leading edge to the outflow. The maximum of each profile is marked with a square marker. Among the 14 abscissa, the locations $x_{H_{12}}, x_d$ and x_{tr} previously defined are highlighted and allow us to make the following observations.

- At $x = x_{H_{12}}$, $\widetilde{u'}_l$ presents a maximum at $\eta_{99} = 0.4$. Fig. 6(b) shows that $\widetilde{u'}_l/\max(\widetilde{u'}_l)$ tends toward the profile predicted by the OPT [30, 29] (excepted outside the boundary layer because the OPT does not take the FST into account). Note that the OPT calculation was done with a 3D compressible code developed by Lucas during his thesis [16]. At the same location, $\widetilde{v'}_n$ and $\widetilde{w'}$ starts to grow.

- At $x = x_d$, $\widetilde{u'}_l$ begins to grow close to the wall, even if the maximum remains located at $\eta_{99} = 0.35$. In Fig. 6(c,d), a maximum inside the boundary layer appears for $\widetilde{v'}_n$ and $\widetilde{w'}$ around $\eta_{99} = 0.5$. These maxima emerge upstream the transition beginning but does not seem related to the streaks themselves, as the streaks have a strong amplitude from $x = -12$cm. These maxima seem correlated to the formation of vortical structures resulting from streak destabilization.

- At $x = x_{tr}$, $\widetilde{u'}_l$ grows rapidly, the position of its maximum is lowered near the wall and the profile gets closer to a turbulent profile. Maxima of the $\widetilde{v'}_n$ and $\widetilde{w'}$ profiles keep lowering and increasing.

From those observations, the time-transverse-averaged flow can be described by breaking it down into three zones. First, a **fully laminar** zone ($x < x_{H_{12}}$) during which streaks are propagating without any instabilities at

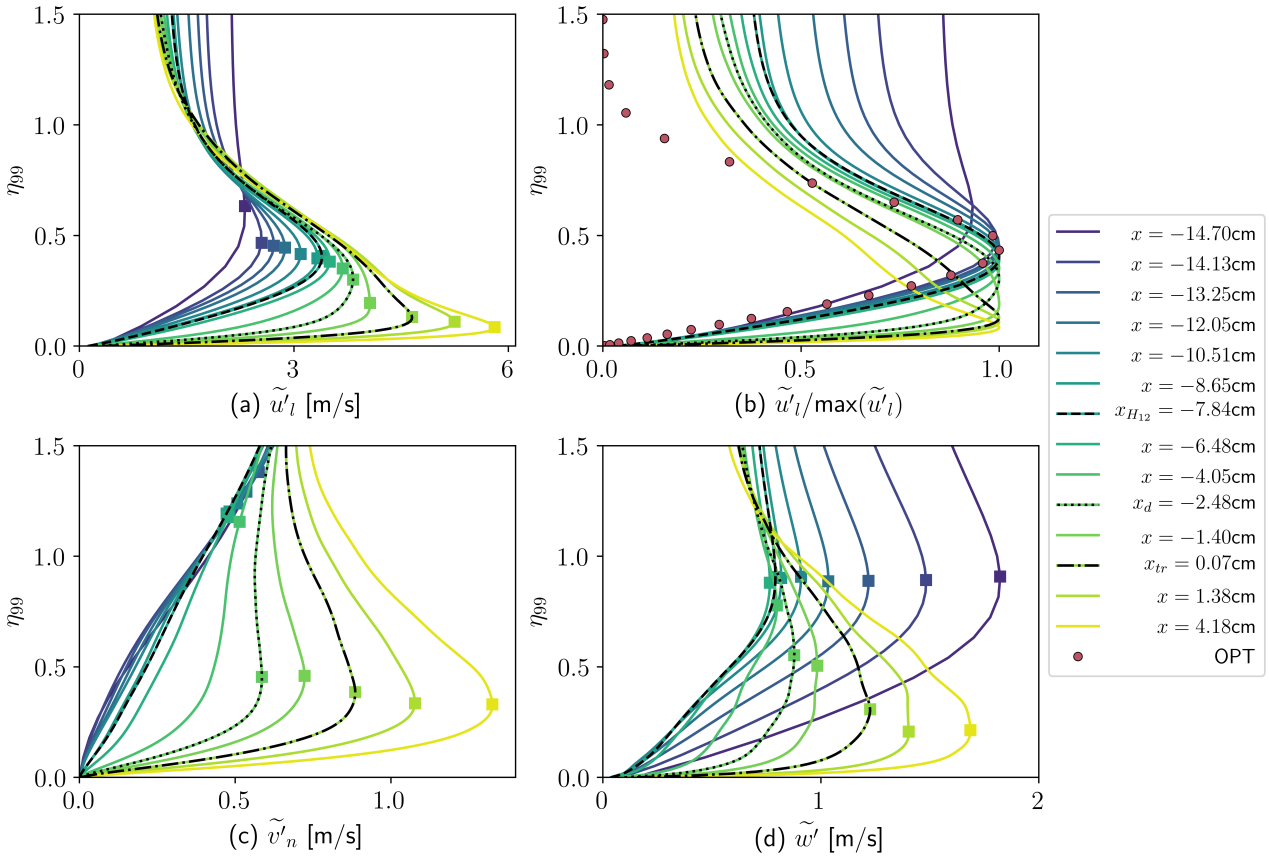

Figure 6: Time-transverse-averaged velocity fluctuation profiles in the boundary layer at several abscissa $x \in [-14.7, 4.18]$ cm. $\widetilde{u'_l}$ is the time-transverse-averaged fluctuation in the streamwise direction, $\widetilde{v'_n}$ in the wall-normal direction and $\widetilde{w'}$ in the transverse direction.

$\eta_{99} \sim 0.4$. Then, a **pre-transitional** zone ($x \in [x_{H_{12}}, x_d]$) during which the wall-normal and spanwise fluctuation component increase until a local maximum appears. In the pre-transitional zone, streaks are destabilized and vortical structures resulting from this destabilization appear. The pre-transitional zone ends with the growth of $\widetilde{u'_l}$ near the wall and the apparition of a local maximum for $\widetilde{v'_n}$ and $\widetilde{w'}$. From this point ($x > x_d$), the flow enters the **transitional zone** where the last streaks are destabilized. The transition is visible on the integral values of the boundary layer at x_{tr} and on velocity fluctuation profiles which are getting closer to fully-turbulent profiles.

3.4 Shear-sheltering

The shear acts as a filter for the external velocity fluctuations penetrating the boundary layer. The boundary-layer receptivity is characterized by strong damping of the high-frequency (or small-wavelength) fluctuations. This phenomenon was named *shear-sheltering* by Jacobs & Durbin [31].

Fig. 7 depicts the Power Spectral Density (PSD) of the streamwise velocity fluctuation u'_l mesured at 5 locations within the boundary layer thickness at $(x,z) = (-7,-0.1)$cm. The frequency range is limited by $f_{min} = 186$Hz and $f_{max} = 7000$Hz. The low-frequency limit f_{min} is imposed by the simulation time. A wave is considered captured by the simulation if 10 periods are calculated:

$$f_{min} = \frac{10}{5.38 \cdot 10^{-2}} = 186\text{Hz}. \quad (2)$$

The high-frequency limit is imposed by the mesh resolution. A wave is considered captured by the simulation if a wavelength is covered by at least 10 cells. This frequency is calculated for each point by taking into account the cell dimensions and the local convection velocity. The high-frequency limit is taken as the lowest f_{max}.

The comparison of these signals in Fig. 7 gives two main information. First, a lot of energy is contained in the low frequencies. The most energetic low frequencies are obtained for $\eta_{99} = 0.4$, which is the height corresponding to the location of streaks in the boundary layer as shown in Fig 5 and is an expected result since streaks are low frequency instabilities. The amplitude of the low frequency fluctuations at $\eta_{99} = 0.4$ is in particular

higher than outside the boundary layer. It means that there is a production of low frequency fluctuations inside the boundary layer. Secondly, Fig. 7 shows that for high frequencies, the PSD level gets lower as η_{99} decreases. In particular, a strong damping of the highest frequencies ($f \geq 2000$Hz) is observed for $y/\delta_{99} = 0.20$ relatively to other boundary-layer heights. This damping is associated with shear-sheltering.

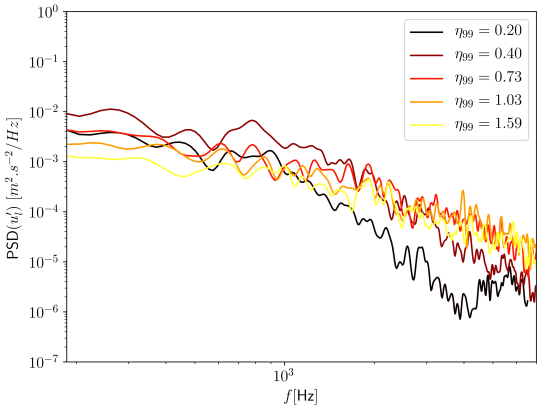

Figure 7: Power Spectral Density of the streamwise velocity fluctuation u_l' at $x = -7$cm, $z = -0.1$cm

Fig. 8 depicts the PSD of u_l' for several abscissa $x \in [-0.14, -0.04]$m, at two boundary-layer heights: (a) $\eta_{99} = 0.2$ and (b) $\eta_{99} = 0.4$. For both boundary-layer heights, the energy level at low frequencies ($f < 600$Hz) is high and is increasing as x moves downward the plate, which is representative of the streaks amplification. Low frequency disturbances (i.e. streaks) are thus produced inside the boundary layer and their amplitude grows with the boundary layer. For high frequencies, the higher levels of energy are found for $x = 0$ and $x = 0.04$, i.e. close to $x \geq x_{tr}$, which is representative of the transition onset.

For $\eta_{99} = 0.20$, the effect of the shear-sheltering is quite clear: the energy level for the high frequencies initially presents at $x = -0.14$m is strongly decreasing as x increases in $[-0.12, -0.07]$, with a cut-off frequency located between 1000 and 2000Hz. The damping is stronger and the cutoff frequency gets smaller when x increases, i.e. when the boundary layer gets thicker. High frequencies start to slowly increase for $x = -0.04$m and reach a higher energetic level for $x \geq 0$. The effect of the shear-sheltering is also visible in Fig. 8b, but the high frequency damping is clearly stronger for $\eta_{99} = 0.2$.

3.5 Klebanoff-mode destabilization

Fig. 9 shows iso-surfaces of the streamwise velocity fluctuation seen from above. Backward (or 'low-velocity') streaks are drawn in black ($u_l' = -4$m/s) and forward (or

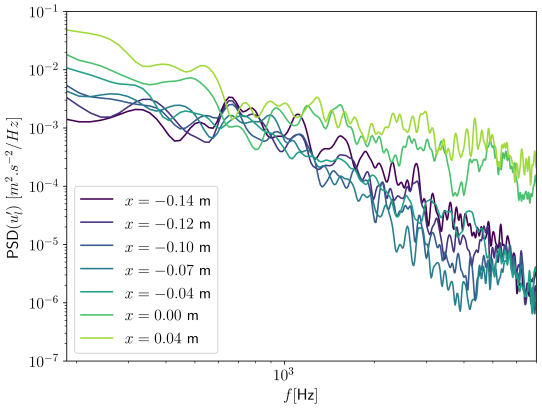

(a) $\eta_{99} = 0.2$

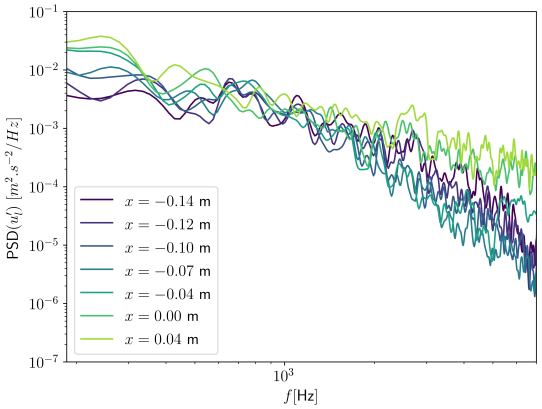

(b) $\eta_{99} = 0.4$

Figure 8: Power Spectral Density of the streamwise velocity fluctuation u_l' at $z = -0.1$cm

'high-velocity') streaks in white ($u_l' = 4$m/s). The leading edge is situated on the left, the flow streams in the right direction. Two images are separated by a physical time of $2.93 \cdot 10^{-4}$s and the time is increasing from above to below. In (a) a backward streak, indicated by a red arrow, presents a sinuous behavior. In (b), vortical structures are enveloping this streak, visible with the Q-criterium iso-surfaces. The sinuous behavior of this streak is more pronounced in (b), (c), and (d). These vortical structures are born at $x \sim -8$cm, which coincides with the beginning of the pre-transitional region where $\widetilde{v'}_n$ begins to grow in the boundary layer in Fig. 6(c). Another backward streak, indicated by a blue arrow, is destabilized in (f) in the transitional zone. Its sinuous behavior is visible from (d). In both cases, destabilized streaks are backward streaks.

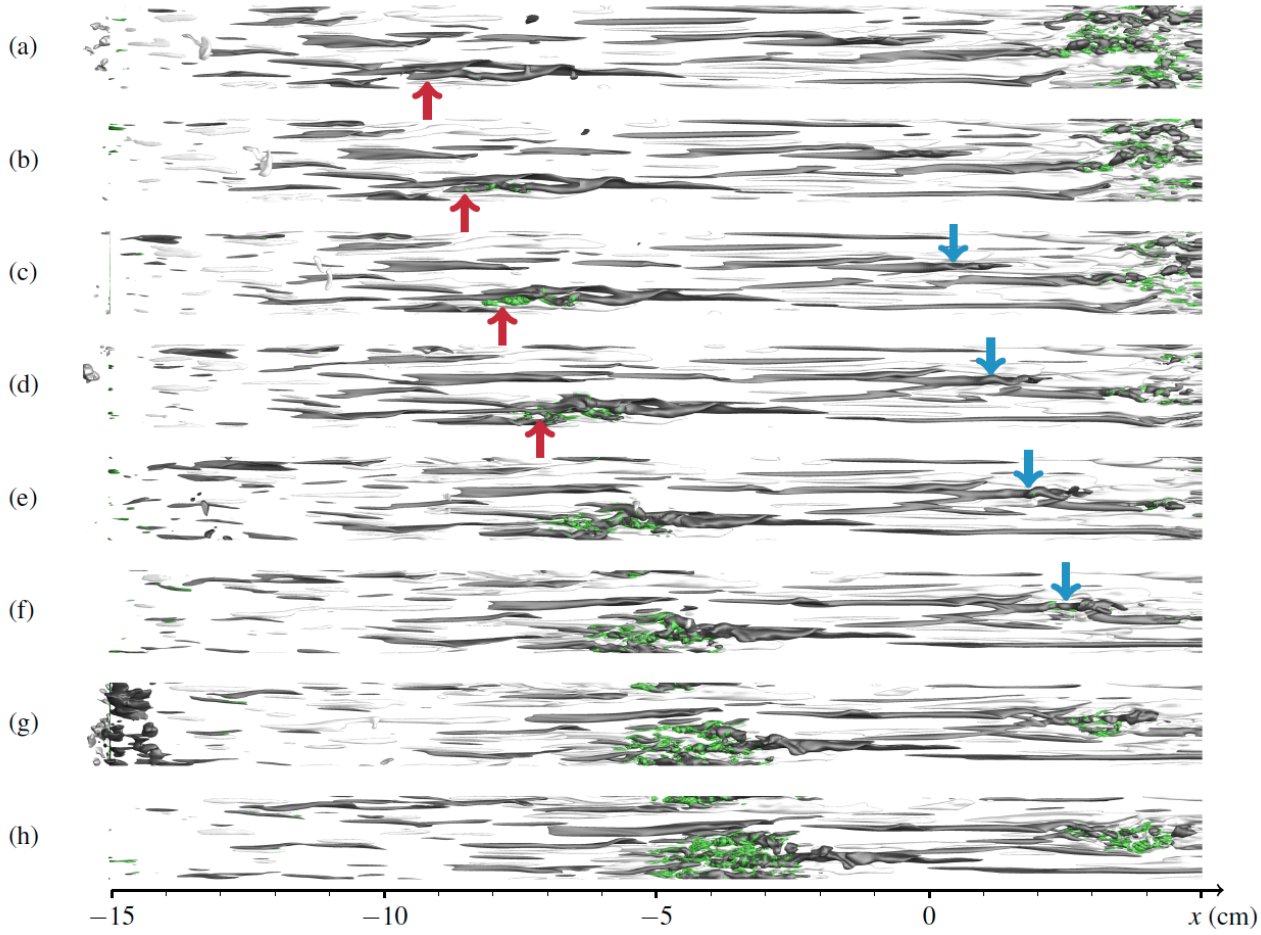

Figure 9: Iso-surfaces of the streamwise velocity disturbances u'_l on the top side of the plate, $u'_l = -4\text{m/s}$ in black, $u'_l = 4\text{m/s}$ in white, and iso-surfaces of Q-criterion in green. The flows comes from the left. Two images are separated by a physical time of $2.93 \cdot 10^{-4}$s (the time is increasing from above to below).

4. CONCLUSION

The amount of data obtained through the LES is very large in terms of averaged quantities, instantaneous snapshots, and time-resolved data at several hundred points in the boundary layer. This amount of data is not fully exploited for now and will probably serve for a certain time for modeling purposes.

Some conclusions regarding this simulation can already be drawn. This simulation is the first to compute a bypass transition flow on a realistic flat plate from the receptivity stage to the Klebanoff-mode destabilization and the beginning of the transition. Both quantitative and qualitative results are valuable for the development of bypass transition models. The LES results are coherent with data from the literature concerning the receptivity region, both in terms of the topology of the vortices exciting the boundary layer and of frequency selection by the shear. The simulated Klebanoff-mode growth shows streamwise fluctuation profiles consistent with the OPT results. Regarding the Klebanoff-mode destabilization, additional post-treatments are needed to better understand the process. At this time, our results do not seem to confirm the scenario proposed by Jacobs *et al.* [9] stating that backward streaks move up in the boundary layer and offer a privileged penetration site for the external turbulence. The instantaneous snapshots should help to clarify this point, in particular by extracting the fluctuations in the $(y,z)-$plane to reveal the presence of secondary instabilities. and confirm the scenario proposed by Brandt *et al.* [10].

One of the most significant results obtained during the data exploitation is the correlation between the increase of the time-transverse-averaged wall-normal velocity fluctuation $\widetilde{v'}_n$ and the first occurrence of the streaks destabilization. The first streaks to be destabilized are located well upstream of the point where the transition is visible on the integral values of the boundary layer and the streamwise velocity fluctuation profile. A pre-transitional zone has been defined ($x \in [x_{H_{12}}, x_d]$) using

the analysis of the time-transverse-averaged flow to describe this region. Observations of the 3D instantaneous data have confirmed the presence of fully-destabilized streaks in the pre-transitional zone. These results offer new prospects for the improvement of the laminar kinetic model developed at ONERA.

ACKNOWLEDGEMENT

This work was granted access to the HPC resources of CINES under the allocation 2018-A0052A10589 made by GENCI.

REFERENCES

[1] P. Klebanoff, "Effect of free-stream turbulence on a laminar boundary layer," *Bulletin of the American Physical Society*, vol. 16, 1971.

[2] J. Kendall, "Experimental study of disturbances produced in a pre-transitional laminar boundary layer by weak freestream turbulence," *AIAA, 18th Fluid Dynamics and Plasmadynamics and Lasers Conference*, 1985.

[3] P. Roach and D. Brierley, "The influence of a turbulent free-stream on zero pressure gradient transitional boundary layer development. Part I: Test cases T3A and T3B," *Numerical simulation of unsteady flows and transition to turbulence*, pp. 319–347, 1992.

[4] P. J. s, O. Mazur, and V. Uruba, "On the receptivity of the by-pass transition to the length scale of the outer stream turbulence," *European Journal of Mechanics-B/Fluids*, vol. 19, no. 5, pp. 707–722, 2000.

[5] M. Matsubara and P. Alfredsson, "Disturbance growth in boundary layers subjected to free-stream turbulence," *Journal of Fluid Mechanics*, vol. 430, pp. 149–168, 2001.

[6] J. Fransson, M. Matsubara, and P. Alfredsson, "Transition induced by free-stream turbulence," *Journal of Fluid Mechanics*, vol. 527, pp. 1–25, 2005.

[7] D. Hernon, E.J.Walsh, and D. McEligot, "Experimental investigation into the routes to bypass transition and the shear-sheltering phenomenon," *Journal of Fluid Mechanics*, vol. 591, no. 461–479, 2007.

[8] P. R. Voke and Z. Yang, "Numerical study of bypass transition," *Physics of Fluids*, vol. 7, 1995.

[9] R. Jacobs and P. Durbin, "Simulations of bypass transition," *Journal of Fluid Mechanics*, vol. 428, pp. 185–212, 2001.

[10] L. Brandt, P. Schlatter, and D. Henningson, "Transition in boundary layers subject to free-stream turbulence," *Journal of Fluid Mechanics*, vol. 517, pp. 167–198, 2004.

[11] S. Nagarajan, S. Lele, and J. Ferziger, "Leading-edge effects in bypass transition," *Journal of Fluid Mechanics*, vol. 572, pp. 471–504, 2007.

[12] V. Ovchinnikov, M. Choudhari, and U. Piomelli, "Numerical simulations of boundary-layer bypass transition due to high-amplitude free-stream turbulence," *Journal of Fluid Mechanics*, vol. 613, pp. 135–169, 2008.

[13] L. Jecker, O. Vermeersch, H. Deniau, E. Croner, and G. Casalis, "A laminar kinetic energy model based on the Klebanoff-mode dynamics to predict bypass transition," *European Journal of Mechanics-B/Fluids*, 2018.

[14] A. Tumin and E. Reshotko, "Optimal Disturbances in Compressible Boundary Layers," *AIAA Journal*, vol. 41, no. 12, pp. 2357–2363, 2003.

[15] O. Vermeersch, *Étude et modélisation du phénomène de croissance transitoire pour des couches limites incompressibles et compressibles*. PhD thesis, ISAE, Toulouse, 2009.

[16] J. Lucas, *Spatial optimal perturbations for transient growth analysis in three-dimensional boundary layers*. PhD thesis, ISAE, Toulouse, 2014.

[17] Y. Daswani, O. Vermeersch, and F. Mery, "A new windtunnel for bypass transition : Design, Manufacturing and Characterization," *56th 3AF International Conference on Applied Aerodynamics*, 2022.

[18] L. Cambier and M. Gazaix, "elsA – an efficient object-oriented solution to CFD complexity," *40th AIAA Aerospace Sciences Meeting & Exhibit*, 2002.

[19] S. Lele, "Compact finite difference schemes with spectral-like resolution," *Journal of Computational Physics*, vol. 103, no. 1, pp. 16–42, 1992.

[20] A. Fosso, *Schémas Volumes Finis précis : application à l'aéroacoustique numérique de jets subsoniques*. PhD thesis, Université Paris VI, 2011.

[21] M. R. Visbal and D. V. Gaitonde, "On the use of higher-order finite-difference schemes on curvilinear and deforming meshes," *Journal of Computational Physics*, vol. 181, no. 1, pp. 155–185, 2002.

[22] C. Bogey and C. Bailly, "A family of low dispersive and low dissipative explicit schemes for flow and noise computations," *Journal of Computational Physics*, vol. 194, no. 1, pp. 194–214, 2004.

[23] C. Tam and Z. Dong, "Radiation and outflow boundary conditions for direct computation of acoustic and flow disturbances in a non-uniform mean flow," *Journal of Computational Acoustics*, vol. 4, no. 2, pp. 175–201, 1996.

[24] T. Poinsot and S. Lele, "Boundary conditions for direct simulations of compressible viscous flows," *Journal of Computational Physics*, vol. 101, no. 1, pp. 104–129, 1992.

[25] W. Bechara, C. Bailly, P. Lafon, and S. Candel, "Stochastic approach to noise modeling for free turbulent flows," *AIAA Journal*, vol. 32, no. 3, pp. 455–463, 1994.

[26] T. von Kármán, "Progress in the statistical theory of turbulence," *Proceedings of the National Academy of Sciences*, vol. 34, no. 11, pp. 530–539, 1948.

[27] L. Brandt and H. D. Lange, "Streak interactions and breakdown in boundary layer flows," *Physics of Fluids*, vol. 20, no. 2, 2008.

[28] M. Landahl, "A note on an algebraic instability of inviscid parallel shear flows," *Journal of Fluid Mechanics*, vol. 98, no. 2, pp. 243–251, 1980.

[29] P. Luchini, "Reynolds-number-independent instability of the boundary layer over a flat surface: optimal perturbations," *Journal of Fluid Mechanics*, vol. 404, pp. 289–309, 2000.

[30] P. Andersson, M. Berggren, and D. Henningson, "Optimal disturbances and bypass transition in boundary layers," *Physics of Fluids*, vol. 11, no. 1, pp. 134–150, 1999.

[31] R. Jacobs and P. Durbin, "Shear sheltering and the continuous spectrum of the Orr-Sommerfeld equation," *Physics of Fluids*, vol. 10, no. 8, pp. 2006–2011, 1998.